The Response of the SSM/I to the Marine Environment. Part II: A Parameterization of the Effect of the Sea Surface Slope Distribution on Emission and Reflection

GRANT W. PETTY

Department of Earth and Atmospheric Sciences, Purdue University, West Lafayette, Indiana

KRISTINA B. KATSAROS

Department of Atmospheric Science, University of Washington, Seattle, Washington

(Manuscript received 30 September 1992, in final form 7 June 1993)

ABSTRACT

Based on a geometric optics model and the assumption of an isotropic Gaussian surface slope distribution, the component of ocean surface microwave emissivity variation due to large-scale surface roughness is parameterized for the frequencies and approximate viewing angle of the Special Sensor Microwave/Imager. Independent geophysical variables in the parameterization are the effective (microwave frequency dependent) slope variance and the sea surface temperature. Using the same physical model, the change in the effective zenith angle of reflected sky radiation arising from large-scale roughness is also parameterized. Independent geophysical variables in this parameterization are the effective slope variance and the atmospheric optical depth at the frequency in question. Both of the above model-based parameterizations are intended for use in conjunction with empirical parameterizations relating effective slope variance and foam coverage to near-surface wind speed. These empirical parameterizations are the subject of a separate paper.

1. Introduction

The launch in June 1987 of the Special Sensor Microwave/Imager (SSM/I) ushered in a new era in the operational and research-oriented use of satellite microwave imagers to observe the marine environment. This instrument senses thermal radiation in both vertical and horizontal polarization at 19.35, 22.235, 37.0, and 85.5 GHz (the 22-GHz channel senses vertical polarization only) and is intended to provide synoptic-scale and meso-α-scale maps over ocean areas of integrated water vapor, integrated cloud liquid water, surface wind speed, and precipitation. While earlier microwave instruments such as the Scanning Multichannel Microwave Radiometer (SMMR) operated in the same spectral band and with five similar or identical channels, the SSM/I offers greatly improved calibration and sampling characteristics (Hollinger et al. 1990) and, for the first time, provides near-real-time microwave imagery to selected operational weather forecasting facilities.

As noted in Part I of this study (Petty and Katsaros 1992), published retrieval algorithms for the SSM/I have either been purely statistical in nature or else have involved the inversion of highly simplified, deterministic models for the dependence of SSM/I brightness temperatures on the scene being observed. A nonlinear physical retrieval algorithm utilizing a more refined brightness temperature model in conjunction with suitable statistical constraints should have at least the potential to yield more accurate results and, perhaps more importantly, to do so over a wider range of conditions than can be accommodated by existing statistical or deterministic algorithms. The development, calibration, and application of an improved brightness temperature parameterization for the SSM/I is therefore the purpose of this paper and its companions.

The modeling of the atmospheric component of SSM/I brightness temperatures was addressed in some detail in Part I. However, because the atmosphere is relatively transparent at SSM/I frequencies, thermal emission and reflection from the surface are almost always important components of the brightness temperatures observed from space. This fact has two important consequences: (i) it is possible to observe variations in the surface emission under most conditions, in principle permitting the observations to be interpreted in terms of the relevant surface variables, and (ii) it is almost always necessary to accurately account for surface variability when attempting quantitative retrievals of atmospheric parameters.

The objective of Part II is therefore to model the effects of large-scale sea surface roughness on observed SSM/I brightness temperatures and to present con-

Corresponding author address: Grant W. Petty, Department of Earth and Atmospheric Sciences, 1397 Civil Engineering Building, Purdue University, West Lafayette, IN 47907-1397.

venient parameterization of these effects. The general theory and qualitative behavior of sea surface emissivity and reflection in the microwave band have been discussed in numerous papers by other authors (Stogryn 1967; Hollinger 1971; Nordberg et al. 1971; Wu and Fung 1972; Webster et al. 1976; Wilheit 1979a; Wilheit 1979b; Wentz 1983; Guissard and Sobieski 1987; Sasaki et al. 1987); here we concentrate on deriving closed-form surface emission and reflection models specifically for the SSM/I's seven channels. As part of this effort, we describe what we believe is an improved approach to the parameterization of reflected sky radiation.

Modeling of sea surface microwave emissivity and bidirectional reflectance entirely from first principles is a problem that continues to challenge theoreticians, both because of the difficulty of measuring and characterizing the shape of the wind-roughened surface and because of the complexity of electromagnetic interactions with any reasonably realistic representation of this shape. It must therefore be emphasized that the following is not a "state-of-the-art" theoretical treatment, nor does it result in a self-contained parameterization of all of the factors affecting the sea surface component of SSM/I brightness temperatures. Rather, the present study focuses on obtaining first-order relationships for those aspects of the sea surface brightness temperature that are difficult to evaluate empirically, particularly the effects of roughness on the magnitude of the reflected sky radiation. These relationships must be supplemented with empirically derived models for the effects of foam, capillary waves, and other factors that do not readily lend themselves to an accurate theoretical treatment. The required empirical components of our sea surface brightness temperature model, as well as empirical adjustments to the atmospheric model derived in Part I, are the subject of Part III of this series of papers.

2. Background

a. *Smooth surface emission and reflection*

In the absence of wind roughening, the sea surface may be modeled as a plane surface bounding a semi-infinite dielectric medium. For electromagnetic plane waves impinging on the interface at an arbitrary angle of incidence θ from normal and with arbitrary polarization, the fraction R of the incident radiation reflected from the interface is then given by the well-known Fresnel formulas:

$$R_V = \left| \frac{\epsilon_s \cos\theta - (\epsilon_s - 1 + \cos^2\theta)^{1/2}}{\epsilon_s \cos\theta + (\epsilon_s - 1 + \cos^2\theta)^{1/2}} \right|^2 \quad (1a)$$

and

$$R_H = \left| \frac{\cos\theta - (\epsilon_s - 1 + \cos^2\theta)^{1/2}}{\cos\theta + (\epsilon_s - 1 + \cos^2\theta)^{1/2}} \right|^2, \quad (1b)$$

where the subscripts V and H refer to vertical and horizontal polarization, respectively, and ϵ_s is the complex dielectric constant of seawater.

By Kirchhoff's law, the thermal emissivity E of the plane surface is given by $(1 - R)$. Hence, the brightness temperature $T_{B,\text{plane}}$ due to thermal emission from the flat sea surface at polarization $p = V$ or H and surface temperature T_S may be written simply as

$$T_{B,\text{plane}} = E_p T_S = (1 - R_p) T_S. \quad (2)$$

To compute E_V and E_H from (1), we use the semi-empirical formula for ϵ_s of Klein and Swift (1977). At SSM/I frequencies, the salinity dependence is very weak. Therefore, one may assume a constant value of $S = 36.5$ ppt in the Klein and Swift formula and restrict one's attention to the effects of viewing angle θ and surface temperature T_S. Figure 1 depicts contour plots of emissivity as a function of T_S and θ for all SSM/I frequencies.

In each case $E_V > E_H$ everywhere, except for $\theta = 0$, for which the distinction between horizontal and vertical polarization disappears, and for $\theta = 90°$, where emissivity is zero for both polarizations. A well-known consequence of this difference is that, in general, for an obliquely viewed ocean surface, microwave brightness temperatures are significantly higher for vertically polarized radiation than for horizontally polarized radiation.

b. *Effects of surface wind roughening*

The action of wind on the ocean surface is known to lead to appreciable deviations of the surface emissivity and reflectivity from those predicted by the Fresnel relations. At the wavelengths observed by the SSM/I, important contributing factors to wind-induced brightness temperature changes include the large-scale distribution of surface slopes, which affects both the scene-averaged Fresnel emissivity and the angular weighting of diffusely reflected sky emission.

Considerably more difficult to model, but also significant, are the radiative effects of features having structure on the scale of the wavelength of the radiation sensed (0.35–1.55 cm for the SSM/I). These include capillary waves, foam and bubbles, and wind-driven spray, all of which are likely to contribute in varying degrees to an increase in surface emissivity.

Satellite-observed microwave surface emissivity is in any case only a rather indirect measure of the wind speed U measured at some standard height above the surface. It is perhaps somewhat more directly indicative of wind stress (or friction velocity), which depends not only on U but also on the thermal stratification of the surface layer of the atmosphere, among other things. Indeed, the roughness and degree of foam coverage to which a microwave radiometer directly responds are further likely to be functions of other variables besides wind stress, including wind fetch and duration, swell,

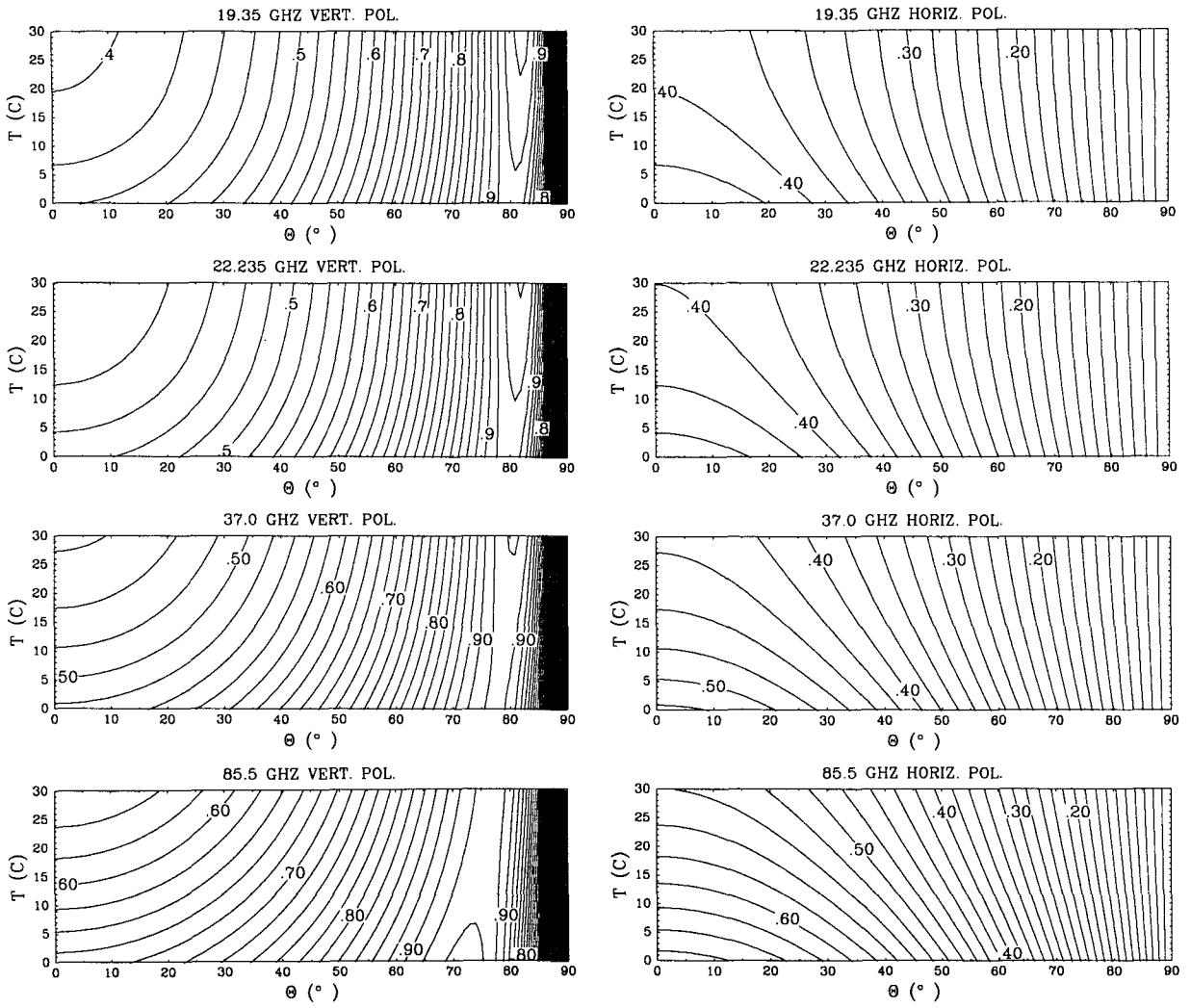

FIG. 1. Fresnel emissivity of seawater (salinity 36.5 ppt) as a function of viewing angle θ and temperature T_S for SSM/I frequencies.

seawater viscosity (which depends on temperature), and surface tension (which is influenced by the presence of organic films). Nevertheless, the generally strong correlation between U and surface emissivity in the microwave spectrum permits one to speak of the "response" of the SSM/I to U, provided only that any quantitative relationship is understood as representing "typical" conditions only.

While the capability of space-borne microwave radiometers like the SSM/I and its forerunner, the SMMR, to provide useful estimates of U has been thoroughly demonstrated by way of several successful statistical or empirically calibrated physical wind speed retrieval algorithms developed for these two sensors (e.g., Lipes et al. 1979; Cardone et al. 1983; Goodberlet et al. 1989; Wentz 1992), the mean relationship between wind speed and surface brightness temperature has not yet been parameterized in sufficiently general and accurate form to permit accurate radiative transfer calculations for the SSM/I. Closed-form emissivity models that were based on physical models calibrated against data from the Seasat SMMR (e.g., Pandey and Kakar 1982; Wentz 1983) did not yield satisfactory results when we attempted to directly adapt them to the viewing angle and frequencies of the SSM/I, especially its 85.5-GHz channels.

Also, although a relatively large number of theoretical and empirical studies have addressed various aspects of the relationship between wind speed and surface brightness temperature at selected frequencies, only Wentz (1983) and Guissard and Sobieski (1987) appear to have addressed the contribution of diffusely reflected sky radiation to satellite-observed radiances.

Formally at least, the key to both the polarized surface emissivity ε_p and the brightness temperature contribution T_B^S from reflected sky radiation lies in the bidirectional reflectance function $r_p(\mu, \phi; \mu', \phi')$, since both ε_p and T_B^S may be obtained from r_p by

means of an integral over the upper hemisphere. Specifically,

$$\varepsilon_p(\mu, \phi) = 1 - \frac{1}{\pi}\int_0^{2\pi}\int_0^1 r_p(\mu, \phi; \mu', \phi')\mu' d\mu' d\phi' \quad (3)$$

and

$$T_B^S(\mu, \phi) = \frac{1}{\pi}\int_0^{2\pi}\int_0^1 r_p(\mu, \phi; \mu', \phi')T_B^{\downarrow}(\mu')\mu' d\mu' d\phi', \quad (4)$$

where $T_B^{\downarrow}$ is the downwelling atmospheric brightness temperature as seen from the surface and $\mu \equiv \cos\theta$. (Because the atmospheric radiance $T_B^{\downarrow}$ is not polarization dependent, it is not necessary to separately specify like-polarized and cross-polarized bidirectional reflectances.) With these definitions, the satellite-observed brightness temperature may be written

$$T_B(\mu) = T_B^{\uparrow}(\mu) + \tau[\varepsilon_p(\mu)T_S + T_B^S(\mu)], \quad (5)$$

where $T_B^{\uparrow}$ gives the upwelling atmospheric brightness temperature and τ is the atmospheric transmittance. Detailed parameterizations of these atmospheric terms are given by Petty and Katsaros (1992).

In practice, a fully adequate specification of r_p over the important range of μ' and ϕ' may be difficult to obtain either theoretically or experimentally, even for a single sea state and viewing direction (μ, ϕ). Furthermore, the required numerical integration of r_p over the upper hemisphere may be difficult to perform accurately on account of a very strong peak in the specular direction—one which increasingly approximates a delta function as surface roughness is reduced under conditions of light wind.

For a practical alternative to this approach, Wilheit (1979b) pointed out that the microwave emissivity of the wind-roughened ocean surface might be adequately represented by a geometric optics model requiring knowledge only of the statistical distribution of surface slopes. Under the geometric optics assumption, it is possible to simply average the specular emissivity over this distribution, "taking care to treat polarization properly and to account for the projection of the facet in the view direction." Wilheit assumed a bivariate Gaussian distribution of slopes with wind speed–dependent variances derived from the sun-glitter observations of Cox and Munk (1954).

Since the geometric optics approximation is strictly valid only when the typical horizontal scales of variability and the radii of curvature are much greater than the electromagnetic wavelength in question, Wilheit employed an "effective" slope variance that was taken to be equal to the Cox and Munk slope variance for microwave frequencies greater than 35 GHz but that was reduced by a factor proportional to frequency below 35 GHz. The use of a reduced slope variance was intended to allow for the fact that interactions involving longer microwave wavelengths should be relatively insensitive to that portion of the slope variance contributed by the smallest roughness elements.

Wilheit does not appear to have used his geometric optics formulation to directly evaluate the sensitivity of the contribution by reflected sky radiation to changes in surface roughness; rather, he assumed that this component was adequately given by $T_B^S = [1 - \varepsilon_r(\theta)]T_B^{\downarrow}(\theta)$. Such an approach does not account for the fact that the reflected sky radiation observed at a viewing angle of θ arrives at the surface from a range of zenith angles distributed asymmetrically about θ, usually leading to a significant intensification of the reflected radiation relative to that computed on the basis of a pseudospecular assumption.

Wentz (1983) recognized the need to model diffusely reflected sky radiation in a more realistic way and proposed an effective surface reflection coefficient of the form $R = (1 + \omega U)(1 - \varepsilon)$ acting on the downwelling sky brightness temperature from the specular zenith angle θ. The constant ω was determined for each channel of the SMMR by way of a least-squares fit to model calculations of surface scattering for a wide range of atmospheric and surface conditions. Despite the improvement that the Wentz model represents, Guissard and Sobieski (1987) have pointed out that the coefficients ω in the Wentz model should more realistically be specified as functions of atmospheric transmittance. This observation is rooted in the fact that the atmospheric optical depth determines the θ dependence of the atmospheric radiance $T_B^{\downarrow}$ appearing in (4).

To parameterize roughness effects on the SSM/I brightness temperatures, we have chosen here to use a geometric optics approach similar to that outlined by Wilheit (1979b). Since that paper did not provide the mathematical/computational details of the model, we shall devote some space to presenting the derivation of our own geometric optics model, which we take to be similar in many or most respects to the Wilheit model. We then shall use computational results from this model to parameterize both roughness-induced emission changes and changes in diffuse reflection in terms of effective slope variance, viewing angle, and sea surface temperature for each SSM/I frequency.

Rather than adopting the modified specular reflectivity model used by Wentz (1983, 1992), we have chosen instead to keep the assumed surface reflectivity R equal to the specular value $(1 - \varepsilon_r)$ and to compute an *effective* zenith angle θ' of the reflected sky emission that may differ markedly from the specular zenith angle θ; that is,

$$T_B^S = [1 - \varepsilon_{r,p}]T_B^{\downarrow}(\theta'). \quad (6)$$

Moreover, we shall explicitly parameterize the functional dependence of θ' on the atmospheric optical depth σ.

3. Geometric optics calculations

a. Rough surface emissivity parameterization

We begin by considering radiation emitted from the ocean surface in the direction described by the unit vector $-\mathbf{k}_0$, where $\mathbf{k}_0$ is the viewing direction toward the surface from the satellite. That is,

$$\mathbf{k}_0 = (\sin\theta\cos\phi, \sin\theta\sin\phi, -\cos\theta), \quad (7)$$

where θ is the satellite nadir angle and ϕ is the azimuthal viewing angle relative to the downwind direction $\mathbf{x}$. (The crosswind and vertical directions correspond to unit vectors $\mathbf{y}$ and $\mathbf{z}$, respectively.)

The observed radiation consists of horizontally polarized and vertically polarized components, as determined by the projection of the electric field vector on the unit vectors $\mathbf{h}$ and $\mathbf{v}$, respectively. These are defined here as

$$\mathbf{h} = \frac{\mathbf{z}\times\mathbf{k}_0}{|\mathbf{z}\times\mathbf{k}_0|} \quad (8)$$

and

$$\mathbf{v} = \frac{\mathbf{k}_0\times\mathbf{h}}{|\mathbf{k}_0\times\mathbf{h}|}, \quad (9)$$

so that $\mathbf{h}$ is both horizontal and normal to $\mathbf{k}_0$, and $\mathbf{v}$ is normal to both $\mathbf{k}_0$ and $\mathbf{h}$.

The unit vector $\mathbf{n}$, which is locally normal to the sea surface, is determined by the x and y components of the sea surface slope at that location:

$$\mathbf{n} = \frac{(-s_x, -s_y, 1)}{[s_x^2 + s_y^2 + 1]^{1/2}}, \quad (10)$$

where

$$s_x = \frac{\partial\eta}{\partial x}, \quad (11)$$

$$s_y = \frac{\partial\eta}{\partial y}, \quad (12)$$

and η is the local height of the sea surface.

In the geometric optics approximation, the apparent vertical and horizontal emissivities ε'_V and ε'_H, as seen by the satellite sensor, are then given by the horizontally and vertically polarized Fresnel emissivities E_V and E_H at the local angle of incidence θ_l, rotated from the local frame of reference into the satellite frame of reference:

$$\varepsilon'_H = c_p E_H(\theta_l) + c_s E_V(\theta_l), \quad (13)$$

$$\varepsilon'_V = c_s E_H(\theta_l) + c_p E_V(\theta_l), \quad (14)$$

where

$$\theta_l = \cos^{-1}(-\mathbf{k}_0\cdot\mathbf{n}), \quad (15)$$

$$c_p = |\mathbf{h}\cdot\mathbf{h}'|^2, \quad (16)$$

$$c_s = 1 - c_p, \quad (17)$$

$$\mathbf{h}' = \frac{\mathbf{n}\times\mathbf{k}_0}{|\mathbf{n}\times\mathbf{k}_0|}. \quad (18)$$

In the above, $\mathbf{h}'$ is analogous to $\mathbf{h}$ but is the horizontal unit vector in a frame of reference having $\mathbf{n}$ as the local vertical. Both $\mathbf{h}'$ and $\mathbf{h}$ are perpendicular to $\mathbf{k}_0$, so (16) gives the cosine squared of the angle of rotation (viewed along $\mathbf{k}_0$) between the satellite and local coordinate systems. Accordingly, (17) gives the sine squared of the same angle.

With the above definitions, it is then straightforward to calculate the effective emissivity ε_r of the roughened surface for each polarization by integrating (13) and (14) over all slopes s_x and s_y, weighted by the probability density $\rho_s(s_x, s_y)$ of those slopes and by a factor $w(s_x, s_y)$, which is related to the viewing geometry:

$$\varepsilon_{rp} = \frac{\int_{-\infty}^{+\infty}\int_{-\infty}^{+\infty}\varepsilon'_p\rho_s w ds_x ds_y}{\int_{-\infty}^{+\infty}\int_{-\infty}^{+\infty}\rho_s w ds_x ds_y}. \quad (19)$$

The geometric factor w must account for both the reduction in solid angle subtended by a sea surface element viewed at an oblique angle and the fact that the probability density ρ_s gives the distribution of slopes referenced to the horizontal projection of each surface element, rather than giving the desired surface *area* distribution as a function of slope. Additionally, w must be set equal to zero when surface elements are viewed from the wrong side. Accordingly,

$$w = \begin{cases} \dfrac{-\mathbf{n}\cdot\mathbf{k}_0}{n_z}, & \text{for } \mathbf{n}\cdot\mathbf{k}_0 < 0 \\ 0, & \text{for } \mathbf{n}\cdot\mathbf{k}_0 \geq 0 \end{cases}, \quad (20)$$

where n_z is the z component of $\mathbf{n}$. Note that in the special case the ocean surface is viewed vertically from above: $w \equiv 1$. Note also that shadowing (i.e., nearby wave surfaces obscuring more distant surfaces) has been ignored here, as its effect on w is both difficult to compute and is probably inconsequential at the SSM/I viewing angle of 53°.

One must consider an additional complication that arises from the fact that, under certain conditions, the apparent emissivity of a facet is due not only to the intrinsic emissivity of the surface at that point but also to reflected emission from other facets. This situation is best examined by considering radiation traveling in the reverse direction, that is, downward along the viewing path in direction $\mathbf{k}_0$. The unit vector giving the direction of the reflected radiation is then

$$\mathbf{k}_s = -2(\mathbf{n}\cdot\mathbf{k}_0)\mathbf{n} + \mathbf{k}_0. \quad (21)$$

When the z component $k_{s,z}$ of this vector is negative, then the scattered ray is downward directed and will encounter the water surface a second time. The total fraction of the original ray that escapes being absorbed is simply the product of the two reflectivities r_1 and r_2, where $r_i \equiv (1 - \varepsilon_i)$. Thus, the combined effective emittance is

TABLE 1. Coefficients for rough ocean surface emissivity model [Eq. (24)].

ν (GHz)	Polarization	C_1	C_2	C_3	C_4
19.35	V	−0.556 + 0	0.357 + 0	−0.312 − 1	0.106 − 1
19.35	H	0.406 + 0	−0.108 + 0	0.128 − 1	0.153 − 2
22.235	V	−0.670 + 0	0.455 + 0	−0.446 − 1	0.232 − 1
22.235	H	0.479 + 0	−0.175 + 0	0.283 − 1	−0.131 − 1
37.0	V	−0.811 + 0	0.551 + 0	−0.365 − 1	0.149 − 1
37.0	H	0.473 + 0	−0.160 + 0	0.312 − 1	−0.150 − 1
85.5	V	−0.723 + 0	0.404 + 0	−0.735 − 2	−0.126 − 1
85.5	H	0.358 + 0	−0.351 − 1	0.309 − 1	−0.121 − 1

$$\varepsilon' = 1 - (1 - \varepsilon_1)(1 - \varepsilon_2), \tag{22}$$

where ε_1 is the emissivity of the first facet encountered and is given by (13) or (14), and ε_2 is the emittance of the second facet and is obtained here by computing the polarization of the reflected ray after the first reflection and then assuming a simple horizontally oriented plane surface for the second reflection. Although the latter assumption is crude, it provides qualitatively reasonable conditions for the second reflection and eliminates the necessity of considering higher-order multiple reflection. Numerical experiments using the above scheme confirmed that the contribution by multiple-reflected radiation is exceedingly small for the SSM/I viewing angle of 53°, so that a more rigorous approach to multiple reflection seems unwarranted.

The one factor in (19) that remains to be specified before one can proceed with numerical calculations is the slope distribution $\rho_s(s_x, s_y)$. Following Cox and Munk (1954), whose conclusions were based on sunglitter pattern observations, ρ_s is generally assumed to be well approximated by a bivariate Gaussian distribution, with downwind and crosswind slope variances g_x^2 and g_y^2, each linearly related to surface wind speed U. However, it is long-standing practice in the microwave sensing literature to ignore the directional dependence of the slope variance and to specify a single slope variance $g^2 = g_x^2 + g_y^2$, so that

$$\rho_s(s_x, s_y) \approx \frac{1}{\pi g^2} \exp\left(-\frac{s_x^2 + s_y^2}{g^2}\right). \tag{23}$$

This simplification was first introduced by Wu and Fung (1972) on the basis of an observed directional insensitivity of emissions from the sea. The figures of Stogryn (1967) indicate that the difference between crosswind and upwind brightness temperature is in fact $\leq$2 K for wind speeds less than 14 m s^{-1} and $\theta = 50°$. Wilheit (1979b) concluded from his own model results that no more than a 2 m s^{-1} error in retrieved wind speed should result from ignoring the effects of anisotropy in the surface emissivity.

The assumption of a direction-independent, Gaussian slope distribution is adequate for the purposes of this study as well. An immediate consequence of this assumption is that the bidirectional reflectance function r_p depends on μ, μ', and $\phi - \phi'$ only, and the rough surface emissivity ε_r depends only on μ.

For each specified surface slope variance g^2, numerical integrations of (19) were carried out for a range of values of sea surface temperature T_S (275, 285, 295, and 305 K) and viewing angle θ (50°, 53°, 56°). Specific values of g^2 corresponded to eight nominal wind speeds (0.2, 2.0, 6.0, 10.0, 14.0, 20.0, 30.0, and 40.0 m s^{-1}) substituted into Wilheit's (1979b) frequency-dependent adaptation of the Cox–Munk relationship. Thus, 96 integrations were performed for each of the four SSM/I frequencies.

The computed rough surface emissivities were expressed as deviations $\Delta\varepsilon_r$ from the Fresnel emissivity for the same parameter values. Standard multiple linear regression was then used to fit the following model to the numerical results obtained for each SSM/I channel:

$$\Delta\varepsilon_r \approx g^2\left[C_1 + C_2\left(\frac{T_S}{273}\right) + C_3(\theta - 53.0) + C_4(\theta - 53.0)\left(\frac{T_S}{273}\right)\right]. \tag{24}$$

The coefficients C_n for each channel are given in Table 1. Maximum absolute errors of the fit occurred for the highest values of g^2 ($\sim$0.2) and ranged from 2×10^{-3} at 19 GHz to 6×10^{-3} at 85 GHz, corresponding to maximum errors in sea surface brightness temperature of $\leq$1 K.

These results are consistent with earlier findings, in that an increase in the effective slope variance g^2 leads to a moderate increase in emissivity for horizontally polarized channels and a slight decrease for vertically polarized channels.

b. *Rough surface reflection/scattering*

Having considered the effect of roughness on the sea surface emissivity, we now turn to the effects of roughness on the sky emission reflected at the surface. Neglecting any azimuthal anisotropy, (4) may be rewritten as

$$T_B^S(\mu) = \frac{1}{\pi}\int_0^{2\pi}\int_0^1 r_p(\mu, 0; \mu', \phi')T_B^{\downarrow}(\mu')\mu' d\mu' d\phi'. \tag{25}$$

Numerical computation of T_B^S using the geometric optics assumption was accomplished in a manner analogous to the rough surface emissivity calculations described above. As noted earlier, the problem is simplified by the fact that atmospheric emission is unpolarized; therefore, we need only integrate (over the distribution of slopes) the local reflectivities multiplied by the atmospheric brightness temperature in the direction from which a ray is reflected by a given surface element toward the satellite sensor:

$$T_B^S = \frac{\int_{-\infty}^{+\infty}\int_{-\infty}^{+\infty} T_B(k_{s,z})(1 - \varepsilon_p')\rho_s w ds_x ds_y}{\int_{-\infty}^{+\infty}\int_{-\infty}^{+\infty} \rho_s w ds_x ds_y}. \tag{26}$$

The indicated integration was performed for the same combinations of values of θ, T_S, and g^2 as for the ε_r calculations. Since reflected radiation from the surface also depends on the intensity and angular distribution of downwelling atmospheric radiation, seven different values of optical depth σ (corresponding to total column water vapor amounts ranging from 0 to 60 kg m^{-2}) and four values of volume absorption coefficient e-folding height (0.5, 1.0, 2.0, and 3.0 km) were used for each combination of surface variables. The downwelling atmospheric radiance $T_B(-\mathbf{k}_s)$ appearing in (26) was computed using the atmospheric parameterization derived by Petty and Katsaros (1992). Altogether, numerical computations of T_B^S were repeated for a total of 21 504 distinct combinations of surface and atmospheric parameters, frequencies, and polarizations.

For each combination of parameters, the effective downwelling brightness temperature $T_B^{\downarrow}(\theta')$ was determined from T_B^S using (6). Figure 2 shows plots of the difference between $T_B^{\downarrow}(\theta')$ and $T_B^{\downarrow}(\theta)$ as a function of atmospheric optical depth and slope variance for the two 85.5-GHz channels. Results are qualitatively very similar for all other SSM/I frequencies. (Here, θ' showed only a very weak dependence on absorption scale height; this dependence is therefore neglected throughout the remainder of this discussion.)

It is apparent that the use of atmospheric radiance from the satellite viewing angle θ as an approximation for the effective atmospheric brightness temperature can lead to errors of order approximately 10 K for reflected radiation observed in horizontal polarization. For vertical polarization, the potential error is smaller, though not necessarily negligible. Interestingly, for each polarization, there is a value of σ for which the difference is zero, and this value is, unexpectedly, nearly independent of g^2. For vertical polarization this value

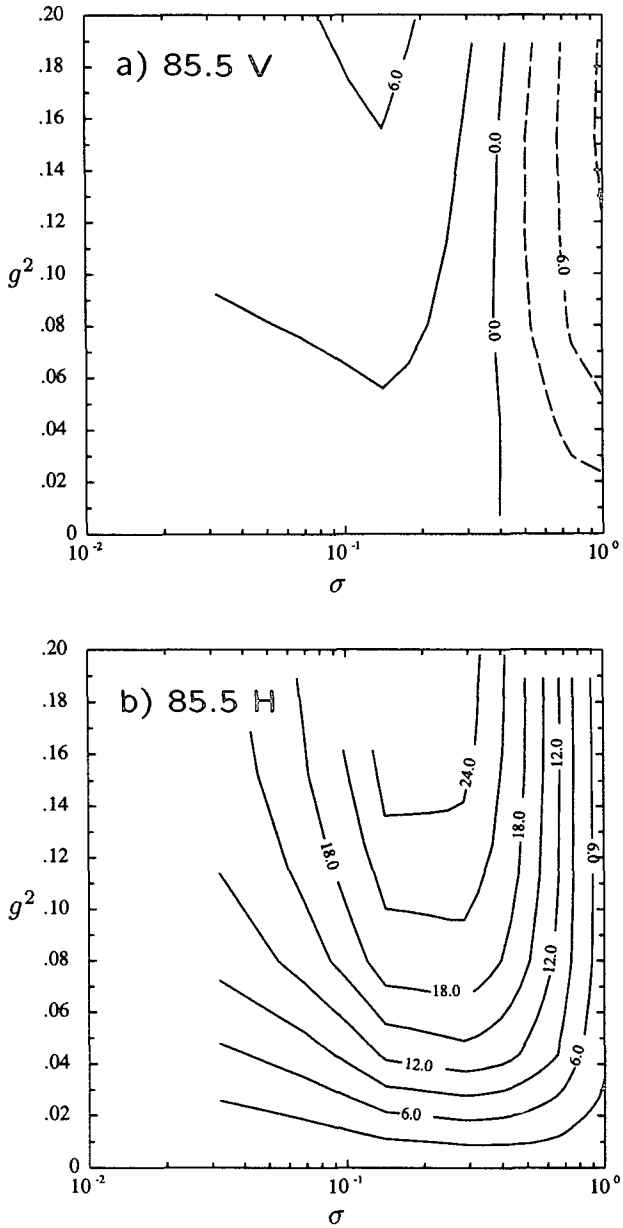

FIG. 2. Plots of $T_B^{\downarrow}(\theta') - T_B^{\downarrow}(\theta)$ as functions of atmospheric optical depth σ and surface slope variance g^2. (a) 85.5 GHz, vertical polarization. (b) 85.5 GHz, horizontal polarization.

of σ occurs near 0.4; for horizontal polarization, it is near 1.3 (not visible in Fig. 2).

Values of $T_B^{\downarrow}(\theta')$ were inverted to obtain θ'. Differences between θ' and the viewing angle of $\theta_0 = 53°$ appear in Fig. 3. The σ dependence of the difference vanishes for $g^2 = 0$, as expected for specular reflection, and the g^2 dependence vanishes for a critical value σ_0 of the optical depth, as already pointed out. Through experimentation, it was also found that, *for fixed slope variance* g^2, $\log(90° - \theta')$ is nearly a linear function of the logarithm of the total atmospheric optical depth.

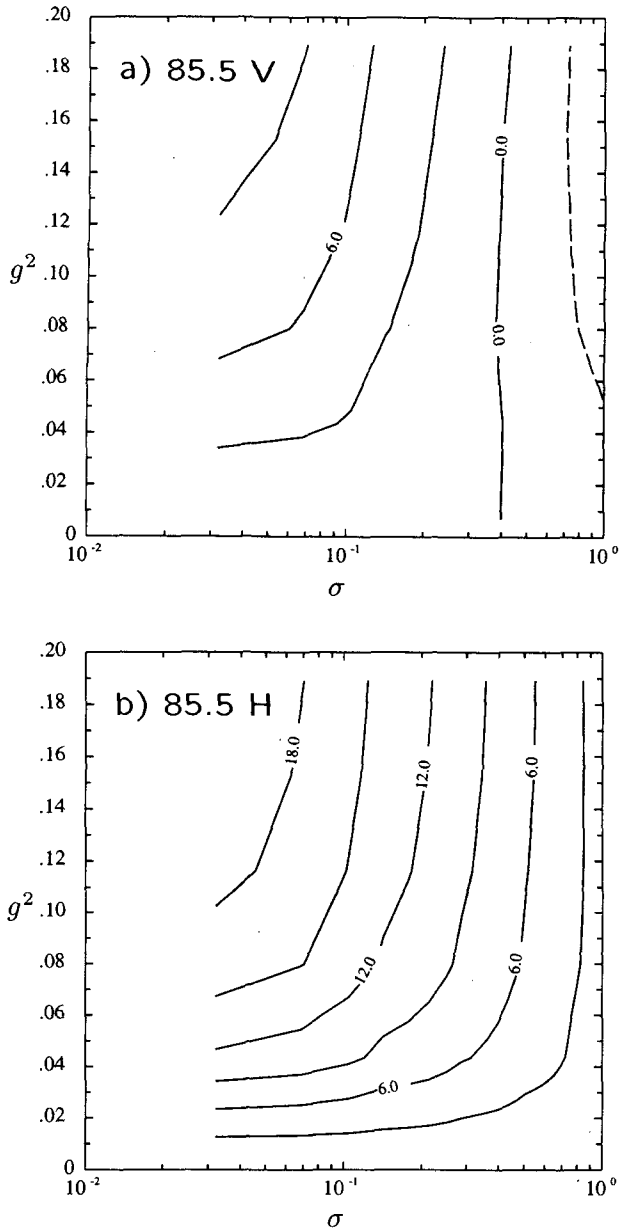

FIG. 3. Plots of $\theta' - \theta$ as functions of atmospheric optical depth σ and surface slope variance g^2. (a) 85.5 GHz, vertical polarization. (b) 85.5 GHz, horizontal polarization.

We therefore used multiple linear regression to find coefficients S_{mn} for a model of the form

$$\frac{90° - \theta_0'}{90° - \theta_0} = \exp\Big[\sum_{m=1}^{2}\sum_{n=1}^{3} S_{mn}(\ln\sigma - c)^m (g^2)^n\Big], \quad (27)$$

where c was determined by inspection of the contour plots.

Each point in the regression was weighted by the squared sensitivity of T_B (as seen from space) to errors in θ', in order to ensure that the fit would be best where accurate values are most needed. Plots of this sensitivity appear in Fig. 4. For very small atmospheric optical depth σ, the brightness temperature sensitivity is small because of weak total emission from the atmosphere; for large σ, the sensitivity is again small because of the low visibility of the ocean surface. The greatest sensitivity of T_B to errors in θ' is therefore at intermediate opacities; that is, $0.1 \gtrsim \sigma \gtrsim 0.4$, for which it may approach 1.0 K per angular degree for a relatively rough surface viewed in horizontal polarization.

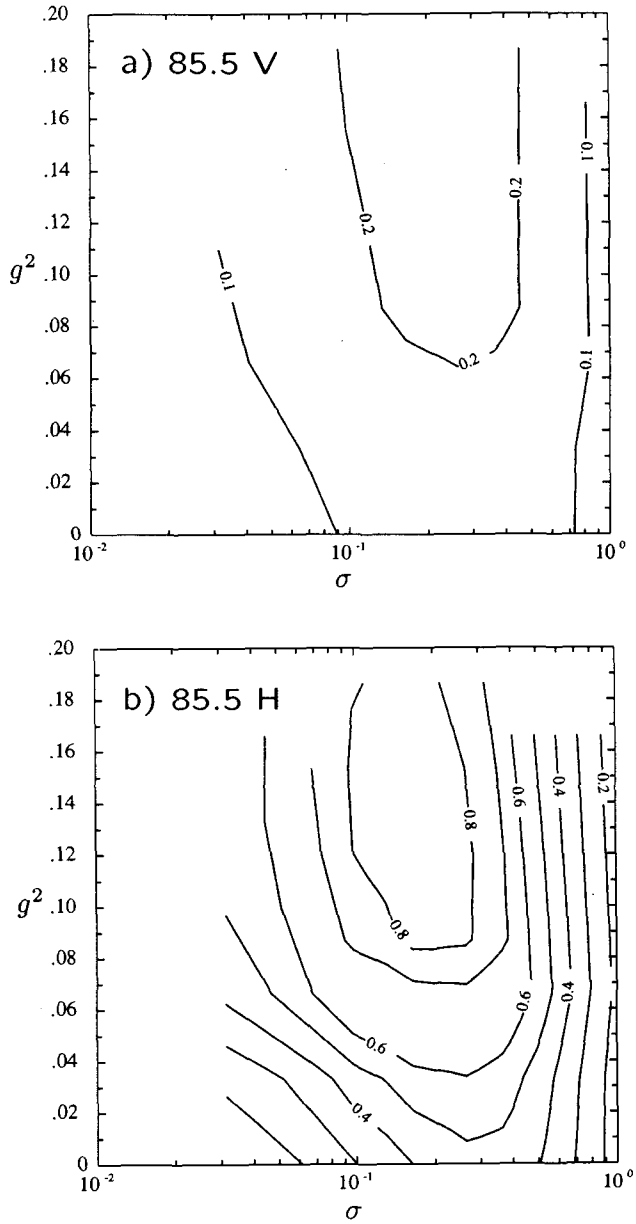

FIG. 4. Plots of $\partial T_B/\partial\theta'$; that is, the sensitivity of computed satellite brightness temperatures to errors in θ', as functions of atmospheric optical depth σ and surface slope variance g^2. (a) 85.5 GHz, vertical polarization. (b) 85.5 GHz, horizontal polarization.

Values of S_{mn} valid for $\theta_0 \equiv 53°$ are given in Table 2. To test the net accuracy of the complete surface model, which consists of (22) and (27) combined with the coefficients in Tables 1 and 2, brightness temperatures observed from space were calculated using both the direct output from the numerical computations for ϵ_r and θ' and the combined model. The differences are plotted for all four SSM/I frequencies and both polarizations in Fig. 5. Maximum absolute brightness temperature errors resulting from the use of the fitted models amount to ≤ 0.5 K for all channels.

Last, we must consider the effect of minor variations in the viewing angle θ on the effective sky radiation angle θ'. For a calm ocean surface, of course, the two are identical. At larger values of g^2, however, the relationship between the two is found to weaken, consistent with the expectation that quasi-specular reflection will gradually give way to quasi-Lambertian scattering (i.e., θ-independent T_B^S) as the roughness increases indefinitely. Since the viewing angle of the SSM/I is confined to a narrow range, only a small, linear correction to the θ'_0 formula obtained for $\theta = 53°$ is necessary to account for other values of θ. This correction is adequately modeled by

$$\Delta\theta' = \begin{cases} (1 - Cg^2)(\theta - 53°), & \text{for } g^2 < 1/C \\ 0, & \text{for } g^2 > 1/C \end{cases} \quad (28)$$

so that

$$\theta' = \theta'_0 + \Delta\theta', \quad (29)$$

where θ'_0 is obtained from (27), and $C \approx 14$ for all frequencies.

4. Summary and discussion

Using a geometric optics model, we have computed and parameterized ocean surface microwave emissivity deviations arising from wind-induced roughness on scales larger than the electromagnetic wavelength. For the frequencies, polarizations, and viewing angle of the SSM/I, our parameterization is given by (24) together with the coefficients presented in Table 1. Independent geophysical variables in this model are the effective slope variance g^2 and the sea surface temperature T_S.

Using the same physical model, we also computed and parameterized the change in the effective zenith angle of reflected sky radiation arising from large-scale roughness. The corresponding formulas and coefficients appear in (27)–(29) and Table 2, respectively. Independent variables are g^2 and the atmospheric optical depth σ.

By computing satellite-observed brightness temperatures using both the raw results of the geometric optics calculations and the above parameterizations of those results, we determined that the latter introduce maximum net brightness temperature errors of no more than about 0.5 K relative to the "exact" results. This is comparable to the nominal sensitivity of the SSM/I instrument itself (Hollinger et al. 1990). Of course, this error estimate applies only to those aspects of the sea surface specifically addressed in the current model.

As has been true of most previous theoretical sea surface microwave emissivity computations, no attempt has been made here to account for the directional dependence of the surface slope spectrum. Rather, we have simply assumed the directionally independent Gaussian slope distribution given by (23). It would of course be straightforward to incorporate separate crosswind and downwind slope variances into the geometric optics model presented here and thus add the relative wind direction as another model parameter. However, a recent empirical investigation of the azimuthal dependence of sea surface emission (Wentz 1992) indicates that the largest difference in observed vertically polarized brightness temperatures is between the upwind and downwind directions, rather than between the upwind–downwind and crosswind directions as would be predicted by a simple Gaussian slope model. Lacking a more suitable description of the slope distribution for now, we have elected to leave the observed directional anisotropy unaccounted for in the present parameterization and regard it (along with other variables) as a modest source of uncertainty in forward calculations of brightness temperature. Future efforts will focus on incorporating empirical parameterizations of this component, starting with the recent results of Wentz (1992), into the complete brightness temperature model described in this set of papers.

TABLE 2. Coefficients for rough ocean surface scattering model [Eq. (27)].

ν (GHz)	Polarization	c	S_{11}	S_{21}	S_{12}	S_{22}	S_{13}	S_{23}
19.35	V	−0.511	2.62	0.402	−23.8	−6.48	69.8	22.5
19.35	H	−0.531	2.91	0.065	−20.6	−1.91	50.7	7.4
22.235	V	−0.511	2.56	0.405	−24.0	−7.14	70.1	24.9
22.235	H	−0.531	2.77	0.008	−19.0	−1.29	44.2	5.0
37.0	V	−0.693	2.53	0.443	−21.1	−6.70	57.3	21.5
37.0	H	−0.182	3.86	0.237	−25.7	−3.02	57.1	8.7
85.5	V	−0.916	1.75	0.270	−10.1	−3.58	26.3	11.6
85.5	H	0.300	3.87	0.196	−25.4	−2.48	56.8	7.4

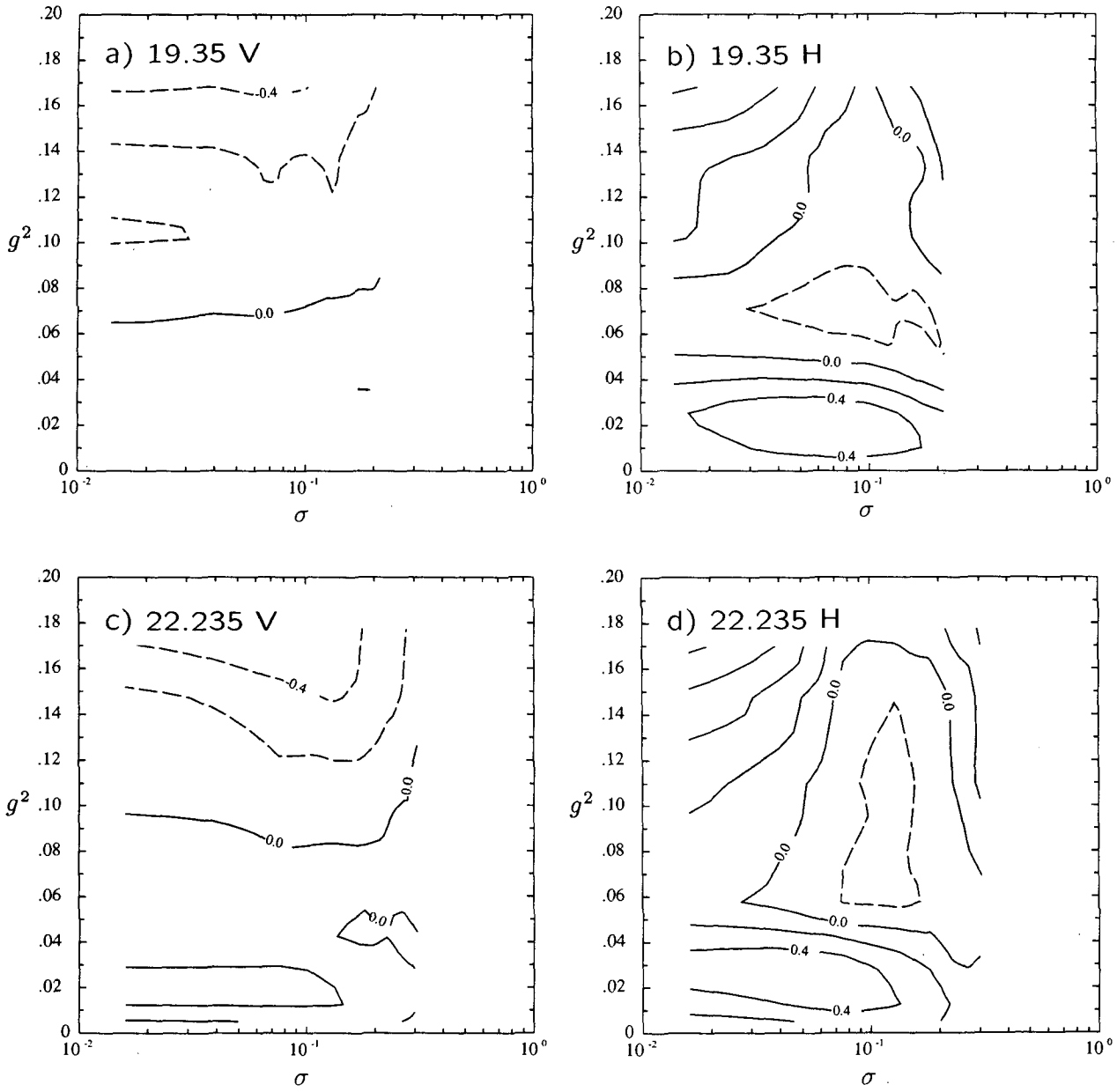

FIG. 5. Net satellite brightness temperature error (K) resulting from the use of fitted models (24) and (27) in place of numerical computations of rough surface emissivity/scattering, for a viewing angle of 53°. (a) 19.35 GHz, vertical polarization. (b) 19.35 GHz, horizontal polarization. (c) 22.235 GHz, vertical polarization. (d) 22.235 GHz, horizontal polarization. (e) 37.0 GHz, vertical polarization. (f) 37.0 GHz, horizontal polarization. (g) 85.5 GHz, vertical polarization. (h) 85.5 GHz, horizontal polarization.

As noted earlier, the independent variable in our parameterization, g^2, is defined here as an *effective* large-scale slope variance that is expected to depend not only on the actual wave structure of the ocean surface (which in turn depends on wind speed, surface-layer stratification, fetch, duration, etc.) but also on the microwave frequency at which the surface is viewed. Also, no attempt has been made in this paper to address the emissivity contribution by factors other than large-scale roughness, such as whitewater or foam. Since neither the mean relationship between g^2, SSM/I frequency, and wind speed nor the dependence of an effective foam coverage on wind speed can be reliably inferred from theoretical considerations alone, the relationship of these variables to SSM/I-observed brightness temperatures remain to be determined empirically in Part III of this study, preliminary results of which have already been presented by Petty (1990).

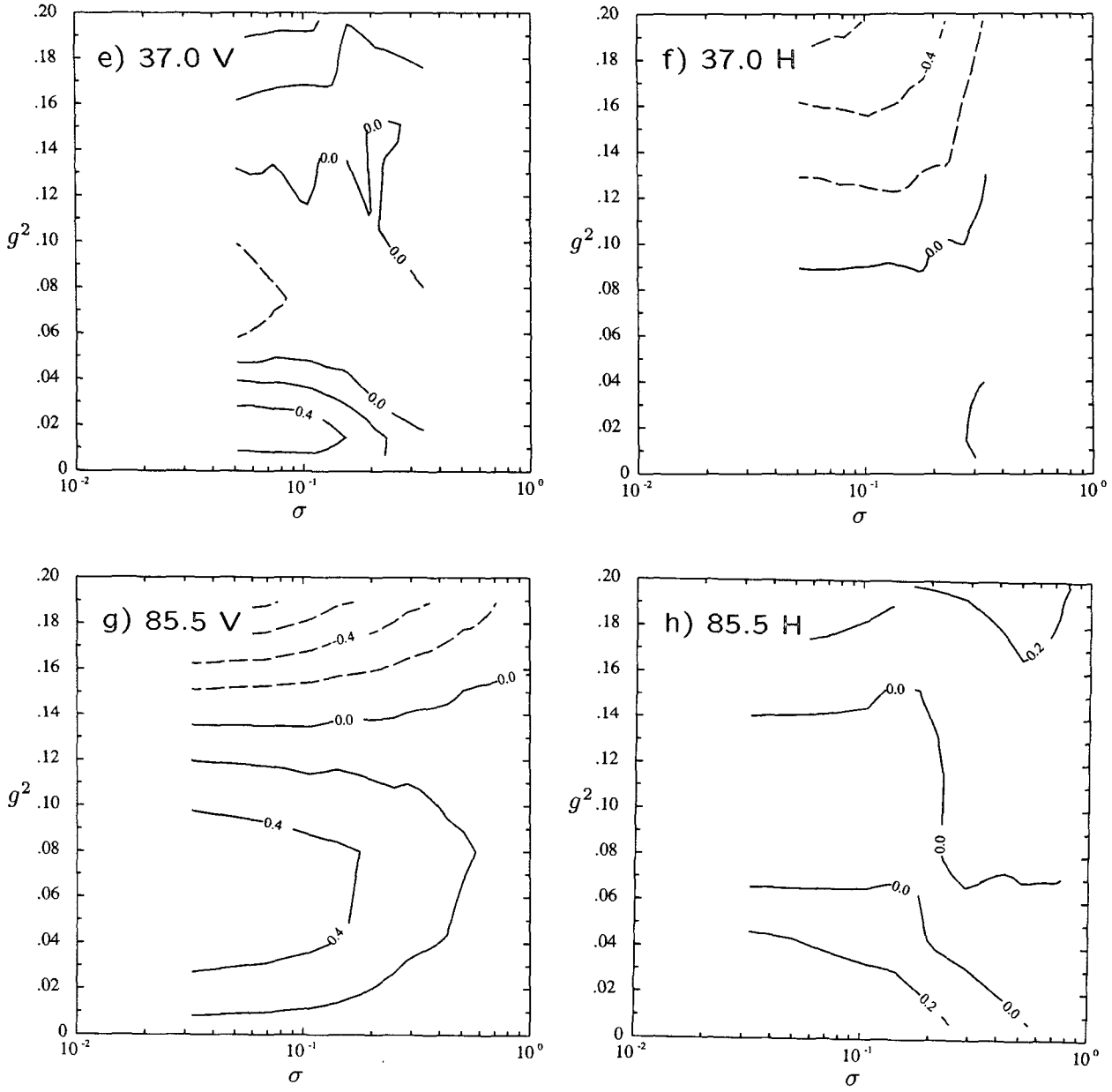

FIG. 5. (*Continued*)

Acknowledgments. This study was performed with support from NASA Grant NAG5-943 to the Department of Atmospheric Sciences at the University of Washington.

REFERENCES

Cardone, V., T. Chester, and R. Lipes, 1983: Evaluation of SEASAT SMMR wind speed measurements. *J. Geophys. Res.*, **88,** 1709–1726.

Cox, C. S., and W. H. Munk, 1954: Measurement of the roughness of the sea surface from photographs of the sun's glitter. *J. Opt. Soc. Am.*, **44,** 838–850.

Goodberlet, M. A., C. T. Swift, and J. C. Wilkerson, 1989: Remote sensing of ocean surface winds with the Special Sensor Microwave/Imager. *J. Geophys. Res.*, **94,** 14 547–14 555.

Guissard, A., and P. Sobieski, 1987: An approximate model for the microwave brightness temperature of the sea. *Int. J. Remote Sens.*, **8,** 1607–1627.

Hollinger, J. P., 1971: Passive microwave measurements of sea surface roughness. *IEEE Trans. Geosci. Electron.*, **9,** 165–169.

——, J. L. Pierce, and G. A. Poe, 1990: SSM/I instrument evaluation. *IEEE Trans. Geosci. Remote Sens.*, **28,** 781–790.

Klein, L. A., and C. T. Swift, 1977: An improved model for the dielectric constant of sea water at microwave frequencies. *IEEE Trans. Antennas Propag.*, **25,** 104–111.

Lipes, R. G., R. L. Bernstein, V. J. Cardone, K. B. Katsaros, E. J. Njoku, A. L. Riley, D. B. Ross, C. T. Swift, and F. J. Wentz, 1979: Seasat scanning multichannel microwave radiometer: Results of the Gulf of Alaska workshop. *Science,* **204,** 1415–1417.

Nordberg, W., J. Conaway, D. B. Ross, and T. Wilheit, 1971: Measurements of microwave emission from a foam-covered wind-driven sea. *J. Atmos. Sci.,* **28,** 429–435.

Pandey, P. C., and R. K. Kakar, 1982: An empirical microwave emissivity model for a foam-covered sea. *IEEE J. Oceanic Eng.,* **7,** 135–140.

Petty, G. W., 1990: On the response of the Special Sensor Microwave/Imager to the marine environment—Implications for Geophysical parameter retrievals. Ph.D. dissertation, University of Washington, 291 pp. [Available from University Microfilms International, Ann Arbor, MI 48106.]

——, and K. B. Katsaros, 1992: The response of the Special Sensor Microwave/Imager to the marine environment. Part I: An analytic model for the atmospheric component of observed brightness temperatures. *J. Atmos. Oceanic Technol.,* **9,** 746–761.

Sasaki, Y., I. Asanuma, K. Muneyama, G. Naito, and T. Suzuki 1987: The dependence of sea-surface microwave emission on wind speed, frequency, incidence angle, and polarization over the frequency range from 1 to 40 GHz. *IEEE Trans. Geosci. Remote Sens.,* **25,** 138–146.

Stogryn, A., 1967: The apparent temperature of the sea at microwave frequencies. *IEEE Trans. Antennas Propag.,* **15,** 278–286.

Webster, W. J., Jr., T. T. Wilheit, D. B. Ross, and P. Gloersen, 1976: Spectral characteristics of the microwave emission from a wind-driven foam-covered sea. *J. Geophys. Res.,* **81,** 3095–3099.

Wentz, F. J., 1983: A model function for ocean microwave brightness temperatures. *J. Geophys. Res.,* **88,** 1892–1908.

——, 1992: Measurement of oceanic wind vector using satellite microwave radiometers. *IEEE Trans. Geosci. Remote Sens.,* **30,** 960–972.

Wilheit, T. T., 1979a: The effect of wind on the microwave emission from the ocean's surface at 37 GHz. *J. Geophys. Res.,* **84,** 4921–4926.

——, 1979b: A model for the microwave emissivity of the ocean's surface as a function of wind speed. *IEEE Trans. Geosci. Electron.,* **17,** 244–249.

Wu, S. T., and A. K. Fung, 1972: A noncoherent model for microwave emissions and backscattering from the sea surface. *J. Geophys. Res.,* **77,** 5917–5929.